Nat Hazards (2016) 81:779–806
DOI 10.1007/s11069-015-2105-z

ORIGINAL PAPER

Quantification of modification of ground motion due to urbanization in a 3D basin using viscoelastic finite-difference modelling

D. Sahar[1] · **J. P. Narayan**[1]

Received: 19 November 2014 / Accepted: 29 November 2015 / Published online: 9 December 2015

Abstract This paper presents the quantification of modification of ground motion due to urbanization in a 3D basin as compared to the free-field motion. The complex interaction effects of basin and city on the ground motion during an earthquake are termed as site–city interaction (SCI) effect in this paper. The cities were developed using 3D building blocks of sixteen-storey (city 1) and eight-storey (city 2) buildings. The analysis, in terms of ground motion perturbation and % reduction in average spectral amplification (ASA) and kinetic energy (KE) as compared to free-field motion, of the simulated responses of the various 3D basin-city models revealed very large role of basin shape, sediment layering, city shape, building type in the city and city density in the SCI effects on the free-field motion. The first spectral amplification peak frequency at the top of the buildings corroborates with the combined fundamental frequency of the building block and sediment deposit in basin. The obtained very large amplification of the order of 49 at the top of a single B8 building may be due to the closeness of the fundamental frequency of the combined basin-building system with the fundamental frequency of the basin and the dominant frequency in the input signal. This was also responsible for the larger % reduction in ASA and KE in city 2 (B8 buildings) as compared to the city 1 (B16 buildings). Based on the analysis of the obtained results, it is concluded that if a city is developed considering into account the building type, city shape and city density as per the basin shape and sediment parameters can be highly beneficial in reducing the earthquake disaster.

Keywords Site–city interaction effects in 3D semi-spherical and trapezoidal basins · City density · City shape and building type effects on ground motion characteristics

✉ J. P. Narayan
jaypnfeq@iitr.ernet.in

D. Sahar
dakshi_sahar@yahoo.com

[1] Department of Earthquake Engineering, Indian Institute of Technology Roorkee, Roorkee 247667, India

1 Introduction

The experimental study, numerical simulations and the observations from the past earthquakes have shown that the ground motion during an earthquake is largely affected by the special site conditions, e.g. basin, basin shape and built urban environment. In past many seismologists studied the variation of the free-field motion in basins due the physical phenomenon like resonance (Narayan et al. 2002), basin-generated surface waves (Bard and Bouchon 1980; Narayan 2005; Chaljub et al. 2010; Semblat et al. 2010), basin-transduced surface waves (Narayan 2012; Narayan and Kumar 2014b) and basement focusing effects (Gao et al. 1996; Narayan and Kumar 2014a). The study of soil-structure interaction (SSI) effects shows that the buildings situated on soil causes diffraction of the incident body waves (kinematic soil-structure interaction) and largely affects the seismic response of the buildings (Merritt and Housner 1954; Wong and Trifunac 1975). Merritt and Housner (1954) showed the lengthening of the natural periods of vibration of the buildings resting on soft soil with a simple numerical experiment. Based on the forced vibration test, Foutch and Housner (1977) inferred that the natural period of vibration of a nine-storey steel-framed building may increase by nearly 50 per cent during the earthquake.

In addition to above, the vibrations induced in the building during an earthquake are transmitted back into the soil (inertial structure-soil interaction) and creates complex patterns of wave interferences (Wong and Trifunac 1975; Wirgin and Bard 1996; Gueguen and Bard 2005). In other word, a considerable inertial structure-soil interaction effects on the free-field motion may occur, particularly in case of heavy structures like nuclear power plants, high-rise buildings and elevated-highways existing on soft soil deposit (Wolf 1985). The first experiment was carried out by Jennings (1970) in order to estimate the ground motion imported in the soil by the building vibrations. A nine-storey Millikan Library Building at the Caltech campus, San Francisco was excited into resonance by two vibration generators on the 9th floor and ground motion was recorded at distances up to a few kilometres from the building. The waveform recorded in the soil was characterized by the building properties. Later on, Kanamori et al. (1991) also observed the effects of high-rise buildings in Los Angeles, excited by atmospheric shock waves generated by the space shuttle Columbia on its return. Stewart et al. (1999) analysed the available earthquake strong motion data to estimate the effects of inertial interaction on structural response for a variety of geotechnical and structural conditions and concluded that the effect of SSI mainly depends on soil to structure stiffness ratio. Gueguen et al. (2000), based on Volvi experiment, reported the radiated motion as 20 and 5 % of the building base motion at distances of two and ten times of the characteristics length of the structure, respectively. Kim et al. (2001) reported that the World Trade Centre (WTC) during the terrorism attack generated a ground motion which was detected up to distances of few kilometres. The inertial soil-structure interaction effects on site response have also been studied based on the analysis of ambient noise (Chavez-García and Cárdenas-Soto 2002; Gallipoli et al. 2004; Cornou et al. 2004). The study of kinematic and inertial soil-structure interaction reveals that both types of interactions might affect the ground motion characteristics and can modify the response of building as well as the neighbouring buildings (Wong and Trifunac 1975; Wirgin and Bard 1996). But, due to the complex multiple interactions between the diffracted waves, it is very difficult to separate out the individual effect during an earthquake excitation.

In the last two decades, several numerical and experimental works focused on the probable influence of large groups of buildings as well as site effects due to subsoil parameters, on the seismic response of the overall system. Wirgin and Bard (1996) considered 2D numerical model to compute the diffraction pattern of surface waves due to the wave field radiated from buildings during the earthquake. Guéguen et al. (2000) analysed the effects of a group of buildings on the free-field motion and called this group effect as 'site–city interaction (SCI)'. Clouteau and Aubry (2001) performed 3D computations based on boundary element models to characterize the SCI in the case of Nice and Mexico city and concluded that the modifications of the incident field occur mainly for soft layered soils. Tsogka and Wirgin (2003) and Groby et al. (2005) studied the seismic response of an idealized 2D city by considering elastic (lossless) and viscoelastic numerical models, respectively, to assess the impact of the diffraction pattern of surface waves under a set of buildings on the response of buildings. Guéguen et al. (2002) described the global city effect using a simplified soil-structure interaction model by adding the single contribution of each building represented by a single oscillator and proposed a simple analytical relation to estimate the expected efficiency of the SCI effects for any city, whereas Boutin and Roussillon (2004) proposed the model by accounts for the multiple interactions between buildings. Kham et al. (2006) and Semblat et al. (2008) reported that the SCI under double-resonance condition can lead to a significant variation of seismic wave field as compared to the free-field motion and concluded that the effects of SCI is beneficial in some parts of the city and detrimental in the other parts of the basin. Recently, Sahar et al. (2015) simulated the SH-wave responses of various viscoelastic site–city models using the finite-difference (FD) method and reported the role of basin shape, city shape, city heterogeneity and city density in SCI effects on ground motion. Taborda and Bielak (2011) also studied SCI effects based on full 3D integration and concluded that the presence of the urbanized area considerably changes the ground motion in the city and in its neighbourhood.

The extensive literature review revealed that most of the studies on the SCI effects on ground motion are limited to the 2D site–city models, and there are only few studies based on the 3D site–city models. It means that there is an urgent need of investigating the SCI effects considering a 3D site–city model. This paper presents the role of basin shape, sediment layering in basin, city density, building type in city and city shape in the 3D SCI effects on the ground motion characteristics. The seismic response and variation of fundamental frequency of single building located at the centre of a semi-spherical (SS) basin, as compared to the assigned one, is also documented. In order to study the 3D SCI effects, 3D buildings are hypothetically inserted into the 3D FD grid in the form of 3D building blocks. The parameters of these building blocks are obtained using the design practices in India, material property and size (height, length and width) of the building. Further, the height of the considered building is taken in accordance with the construction practices in northern part of India lying in seismic zone IV (IS 1893 (Part 1) 2002).

2 Salient features of the used computer program

A computer program developed by Narayan and Sahar (2014) is used for the simulation of 3D viscoelastic seismic responses of the various site–city models. This program is based on the fourth-order staggered-grid FD approximation of the 3D viscoelastic wave equations, which are developed using the generalized Maxwell body-Emmerich and Korn (GMB-EK) rheological model (Emmerich and Korn 1987). A material independent anelastic function

developed by Kristek and Moczo (2003) was used since it is preferable in case of material discontinuities. The effective values of the density and unrelaxed modulus of rigidity at the required position in FD grid cell are obtained using the arithmetic and harmonic means, respectively (Moczo et al. 2002). An improved vacuum formulation proposed by Zeng et al. (2012) is used as a free surface boundary condition. Zeng et al. (2012) reported that the improved vacuum formulation fully satisfies the free surface boundary condition by using an appropriate combination of the staggered-grid and a parameter averaging scheme proposed by Moczo et al. (2002). The sponge absorbing conditions are implemented on the model faces to avoid the edge reflections (Israeli and Orszag 1981; Kumar and Narayan 2008).

3 The site–city models

To study the SCI effect on the free-field motion 8-stories (B8), 12-stories (B12) and 16-stories (B16) buildings situated in basin are considered. In the numerical model, buildings are represented by homogeneous building blocks in place of the real buildings. The mechanical properties of the homogeneous building block are given in Table 1. The details of finding the time period of the considered buildings as per IS:1893 code as well as fixing the same based on the output of the SAP-15 analysis are given by Sahar et al. (2015). On an average the F_0 of the considered B16, B12 and B8 buildings is taken as 0.62, 0.86 and 1.20 Hz, respectively. The computed fundamental frequency of buildings is used to compute the effective S-wave velocity for the building block model to be incorporated in the numerical grid in place of the real building. The effective shear wave velocity inside the building block model computed using a simple relation $V_s = 4HF_0$ are 119, 124 and 120 m/s for B16, B12 and B8 buildings, respectively. For the simplification, we take S-wave velocity 120 m/s for all the building types. Value of quality factors for waves in the building block model is taken as 10 (for 5 % damping) in RC structures (IS 1893: 2002). Two types of homogeneous cities namely city 1 (consisting of only B16 buildings) and city 2 (consisting of only B8 buildings) are considered. A building block is consisting of four similar buildings. The dimensions (length and width) and heights of the B16 and B8 building blocks and other parameters are given in Table 1. The total area covered by the homogeneous cities is 776 × 776 m^2. The city density for both the cities is 0.42. The city density can be computed using a simple relation

$$\text{City-density (CD)} = \frac{N \cdot W_b \cdot L_b}{W_c \cdot L_c}$$

where N is the number of buildings, W_b and L_b are the width and length of a building, respectively, and W_c (776 m) and L_c (776 m) are the width and length of city, respectively.

Table 1 The different parameters for the buildings

Buildings	B8	B12	B16
Height	24 m	36 m	48 m
Plan (width × length)	20 m × 20 m	24 m × 24 m	28 m × 28 m
Frequency (f_o)	1.20 Hz	0.86	0.62 Hz

So, the number of buildings in regular homogeneous city 1 and city 2 is 324 and 452, respectively, for a city density 0.42. In order to study the SCI effect, two types of basin namely semi-spherical (SS) basin with circular free surface (radius 752 m) and trapezoidal (TRP) basin with square free surface (side 1328 m × 1328 m) are considered. The SS and TRP basins have same free surface area. The slope of the inclined base of the TRP basin is taken as 30°. The maximum depth of sediment in both the basins is 150 m. Figure 1a, b shows the SS and TRP basin models, respectively, with homogeneous city 1 centred at the centre of the basins. There are nine sectors each having nine blocks. Each block, as shown in Fig. 1a, consists of four B16 building blocks. So, finally there are 324 B16 buildings in

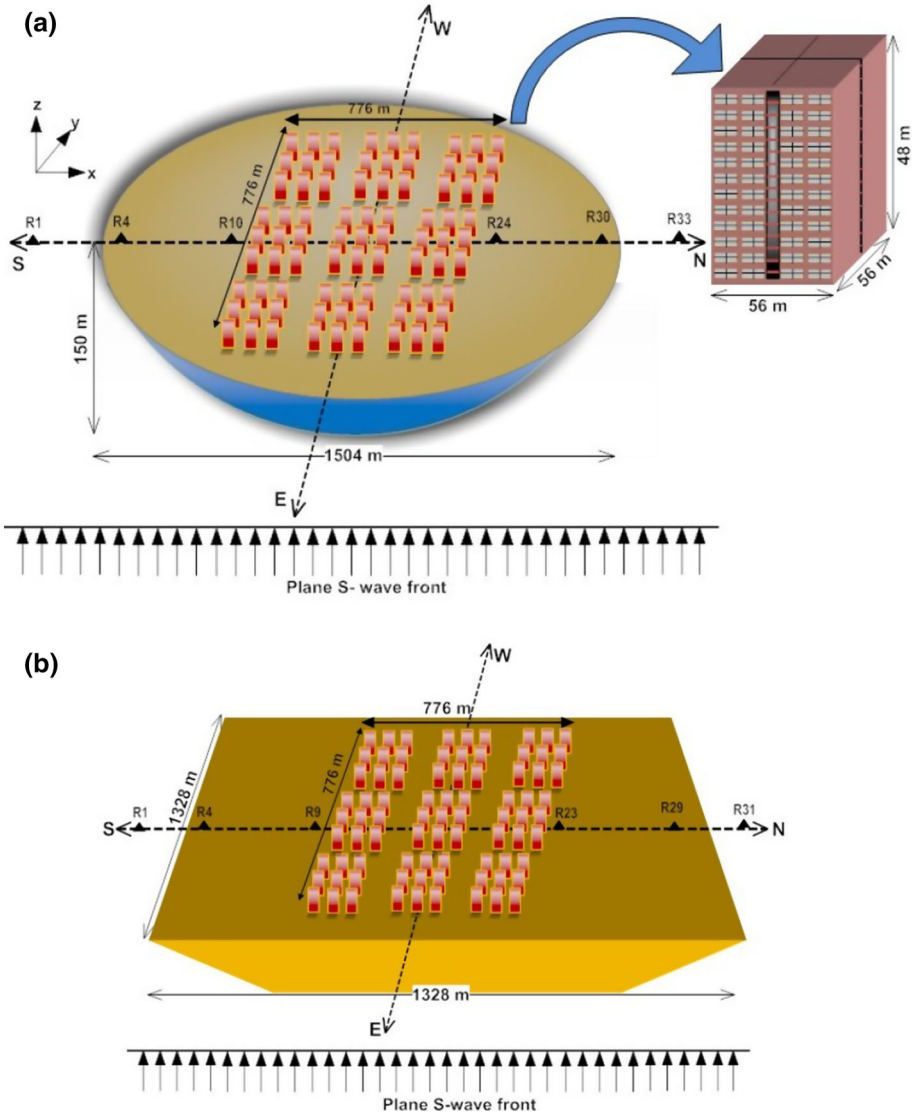

Fig. 1 **a** and **b** The site–city models for homogenous city 1 situated in SS and TRP basins, respectively

the homogeneous city 1. In order to compute the anelastic coefficients, the quality factors for the S- and P-waves are taken as 10 % of the respective velocities at the reference frequency of 1.0 Hz. The P- and S-wave velocities and quality factors at reference frequency 1.0 Hz, density and unrelaxed moduli for the building blocks, sediment and basement rock are given in Table 2.

The site city model is excited by vertically propagating plane S-wave front with the NS polarization. The plane S-wave front with NS polarization is generated using various point sources at a particular horizon. Each point source is generated using shear stress σ_{xz} in the form of Ricker wavelet. Ricker wavelet with dominant frequency 0.6 Hz and upper cut-off frequency around 1.5 Hz is used as a source excitation function. The numerical model is descritized with grid size of 8.0 m in the horizontal directions and 6.0 m in the vertical direction. Further, the time step is taken as 0.00092 s to avoid the numerical instability of the explicit FD scheme used (Narayan and Sahar 2014). Two receiver arrays along north–south (NS) and east–west (EW) directions passing through the centre of basin were used to record the different components of the particle velocity (Fig. 1). Each receiver array consists of 33 receiver points at the free surface at an interval of 56 m. For example, NS array extends 896 m south to 896 m north of the centre of the SS basin.

4 Single building in the SS basin

First, seismic responses at the bottom and top of the single B16, B12, and B8 building situated at the centre of the SS basin were computed to infer the ground motion amplification at the top of the buildings and the effective fundamental frequencies (F_0). A comparison of NS component of the ground motion at the top and the base of the single B16, B12 and B8 building at the centre of the SS basin are shown in Fig. 2a. This figure reveals the increase in duration of ground motion at the top of all the considered buildings. A considerable increase in amplitude at the top of B8 building and a small reduction in amplitude at the top of B16 and B12 buildings can be observed. Figure 2b shows the comparison of spectral amplifications at the base of B16, B12 and B8 buildings with respect to the free-field motion at the exposed rock (no basin in the model). It appears that the spectral amplifications peaks are governed by the resonance modes of the SS basin. A minor reduction in spectral amplifications due to the SCI effect can be inferred. A close analysis shows that the reduction in spectral amplifications due to the SCI is largest at the base of B8 building, and it is somewhat similar at the base of other considered buildings.

Figure 2c shows the spectral amplifications at the top of the considered buildings with respect to the free-field motion at the exposed rock. The obtained first spectral amplification peak frequencies are very much corroborating with the fundamental frequency of the material between the top of the building and the base of the sediment in basin,

Table 2 Parameters for the building blocks, sediment in basin and basement rock

Material	V_S (m/s)	V_P (m/s)	Q_s	Q_P	Density (kg/m^3)	μ_u (GPa)	λ_u (GPa)	K_u (GPa)
Building Block	120	204	10	10	355	0.006	0.005	0.017
Basin	360	612	36	61	1800	0.253	0.201	0.707
Rock	1800	3060	180	30	2650	8.726	7.598	25.052

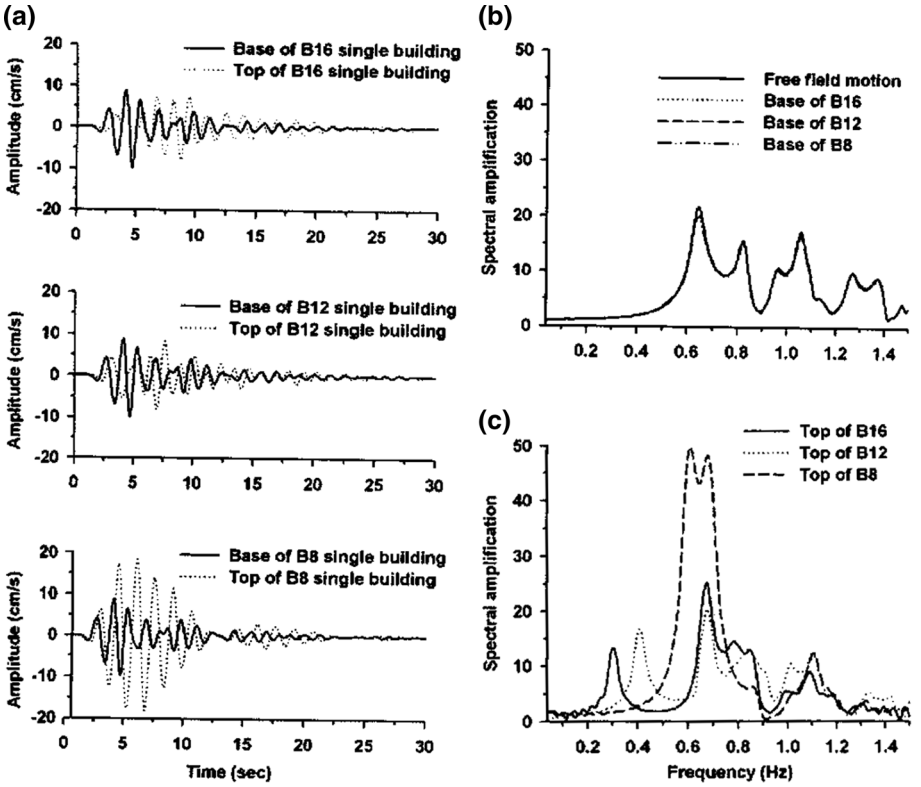

Fig. 2 **a** Comparison of seismic responses at the base and top of a single B16, B12 and B8 building placed at the centre of the SS basin, **b** comparison of spectral amplifications at the base of a single B16, B12 and B8 building with respect to the free-field motion and **c** comparison of spectral amplification at the top of B16, B12 and B8 building

particularly in case of the B16 and B12 buildings. However, in case of B8 building, it is occurring at somewhat higher frequency. The second spectral amplification peak frequency is occurring very near the fundamental frequency of the basin. However, in case of B8 building, very large spectral amplification is occurring with two spectral peaks near 0.62. It may be due to the closeness of the fundamental frequency of the combined basin-building system with the fundamental frequency of the basin and the dominant frequency in the input signal. Theoretically, the largest spectral amplification should occur in case of the B16 building since the assigned fundamental frequency for B16 building was matching with the fundamental frequency of the basin.

A comparison of spectral amplifications at the top of a single B16 and B8 building situated at the centre of the SS basin with the same at the top of building situated at the centre of city 1 and city 2 is shown in Fig. 3a, b, respectively. A reduction in spectral amplifications above the lowest natural frequency of the SS basin at the top of central building of both the homogeneous city 1 and city 2 as compared to the single B16 and B8 building situated at the centre of the SS basin can be inferred. This observation depicts that the reduction in the spectral amplifications is due to the SCI effect. The largest percentage reduction in spectral amplification is around 37.5 % at the top of B16 building in

homogeneous city 1 at 0.68 Hz as compared to the single B16 building in the SS basin. On the other hand, the largest reduction is 44.2 % at the top of B8 building in homogeneous city 2 at 0.64 Hz, whereas the % reduction in spectral amplification at the natural frequency of basin (0.6 Hz) is 8.6 and 39.5 % for homogeneous city 1 and city 2, respectively. The larger reduction in case of city 2 may be due to the closeness of the fundamental frequency of the combined basin-building system with the fundamental frequency of the basin.

5 Effects of basin shape and city type

The seismic responses of the SS and TRP basins in the presence and absence of the homogeneous city 1 and city 2 were computed on both the NS and EW arrays using the incident plane S-wave front with the NS polarization. Figure 4a–c depicts the comparison of responses of the SS basin with (dotted line) and without (solid line) homogeneous city 1 in the NS components on the NS array, NS components on the EW array and UD components of the NS array, respectively. The other components along the NS and EW arrays have no signal. Although both the Love and Rayleigh waves have been generated all along the periphery of the SS basin (the details of the BGS waves generation in the SS basin is given in Kamal and Narayan 2015) along the NS and EW arrays only Rayleigh and Love waves have been generated. This is the reason why there is no signal in the EW components of the NS array and EW and UD components of the EW array. The focusing of the BGS waves may be the reason behind an increase in amplitude of the BGS waves towards the centre of the SS basin. Similarly, Fig. 5a–c depicts the comparison of responses of the SS basin with (dotted line) and without (solid line) homogeneous city 2 in the NS components on the NS array, NS components on the EW array and UD components of the NS array, respectively. A comparison of Figs. 4 and 5 depicts the considerable effects of SCI mainly on the body wave multiples and the BGS waves and their multiples (Fig. 6). A comparison of the seismic responses in the NS components of NS array, NS components of EW array and UD components of NS array of the TRP basin with (dashed line) and without homogeneous city 1 and city 2 (solid line) is shown in Figs. 7 and 8, respectively. In the

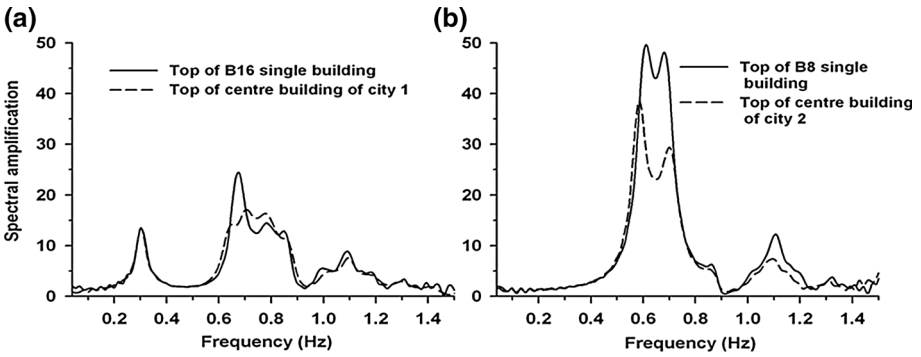

Fig. 3 **a** A comparison of spectral amplifications at the top of a single B16 building with the same at the top a building of a homogeneous city 1 situated at the centre of SS basin and **b** a comparison of spectral amplifications at the top of a single B8 building with the same at the top a building of a homogeneous city 2 situated at the centre of SS basin

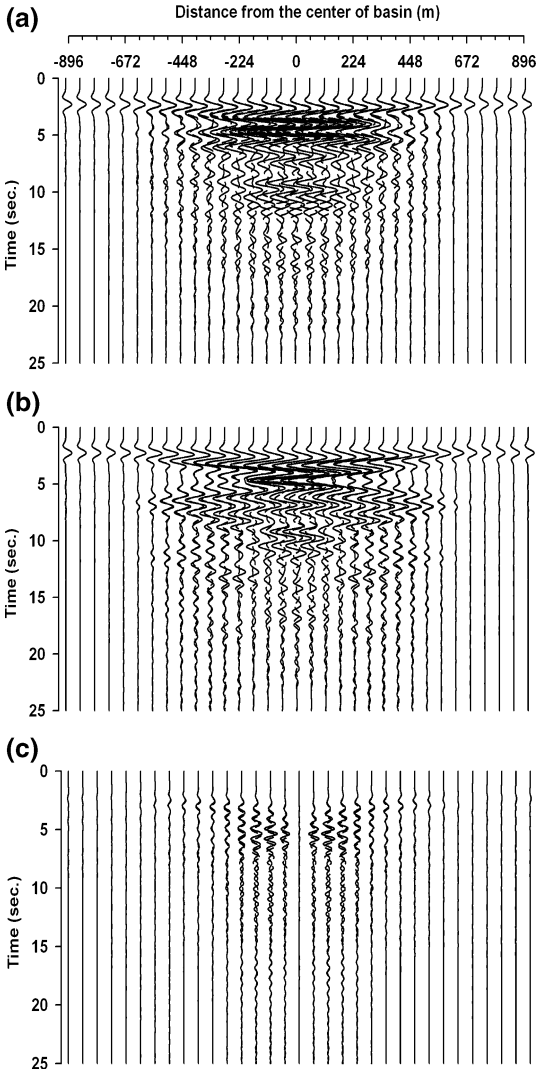

Fig. 4 A comparison of ground motions in different components corresponding to with (*dashed line*) and without (*solid line*) homogenous city 1 in SS basin. **a** NS component of NS array. **b** NS component of EW array. **c** UD component of NS array

trapezoidal basin, the slant part of the base of the basin may play major role in the surface wave generation. The Rayleigh and Love waves will be generated at edges oriented in the EW and NS directions, respectively. The interference of the BGS waves may be responsible for the increase in amplitude of the BGS waves in the central part of the TRP basin. The analysis of Figs. 4, 5, 7 and 8 reveals that there is remarkable effect of basin shape on the free-field motion. But, due to the small depth of the basin, body waves, surface waves and body wave multiples cannot be separate out in the time response. To distinguish the role of basin shape, the average spectral amplification (ASA) of each trace has been computed (traces not shown here). The analysis of ASA reveals more amplification in the SS basin in the central part than in the TRP basin. This may be due to the large amplification of ground motion caused by the focusing of the BGS waves in the central part of

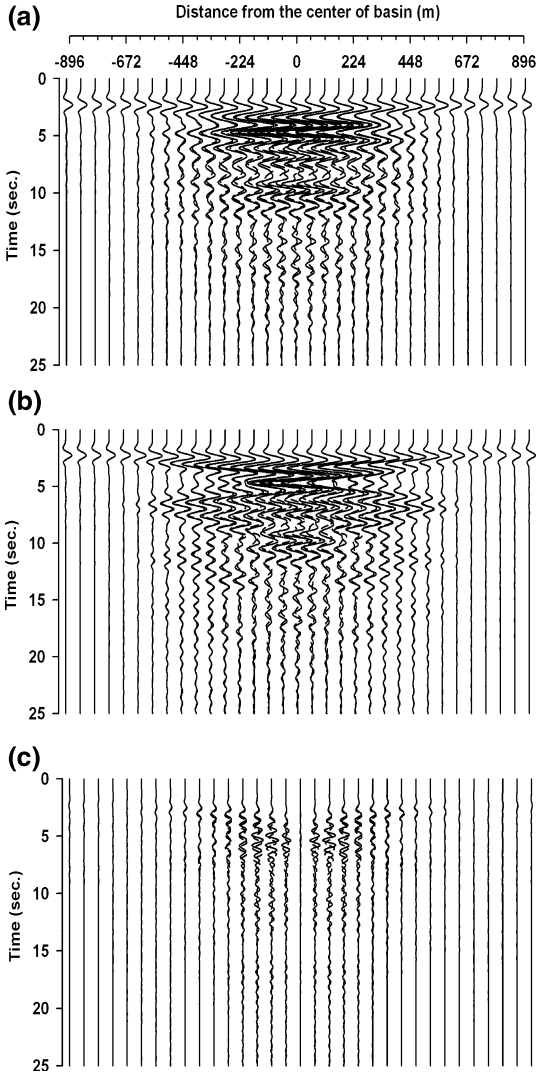

Fig. 5 A comparison of ground motions in different components corresponding to with (*dashed line*) and without (*solid line*) homogenous city 2 in SS basin. **a** NS component of NS array. **b** NS component of EW array. **c** UD component of NS array

the SS basin. To further recognize the role of basin shape in SCI effects, perturbations were also computed for both the homogeneous city 1 and city 2 situated in the SS and TRP basins, as shown in Figs. 6 and 9, respectively. The perturbations were computed just taking the difference of response of basin with and without city. The analysis of Figs. 6 and 9 reveals that the ground motion is highly variable with the shape of basin and the city type. Furthermore, the large perturbation in the NS components along the EW array in the TRP basin reveals larger amplitude of the Love waves in the TRP basin. The perturbation due the city 1 and city 2 is appearing to be comparable in the SS basin and more in city 2 in the TRP basin.

To quantify the role of basin shape in SCI effects on the ground motion in a quantitative way, a comparison of spectral amplifications in the NS components along the NS array

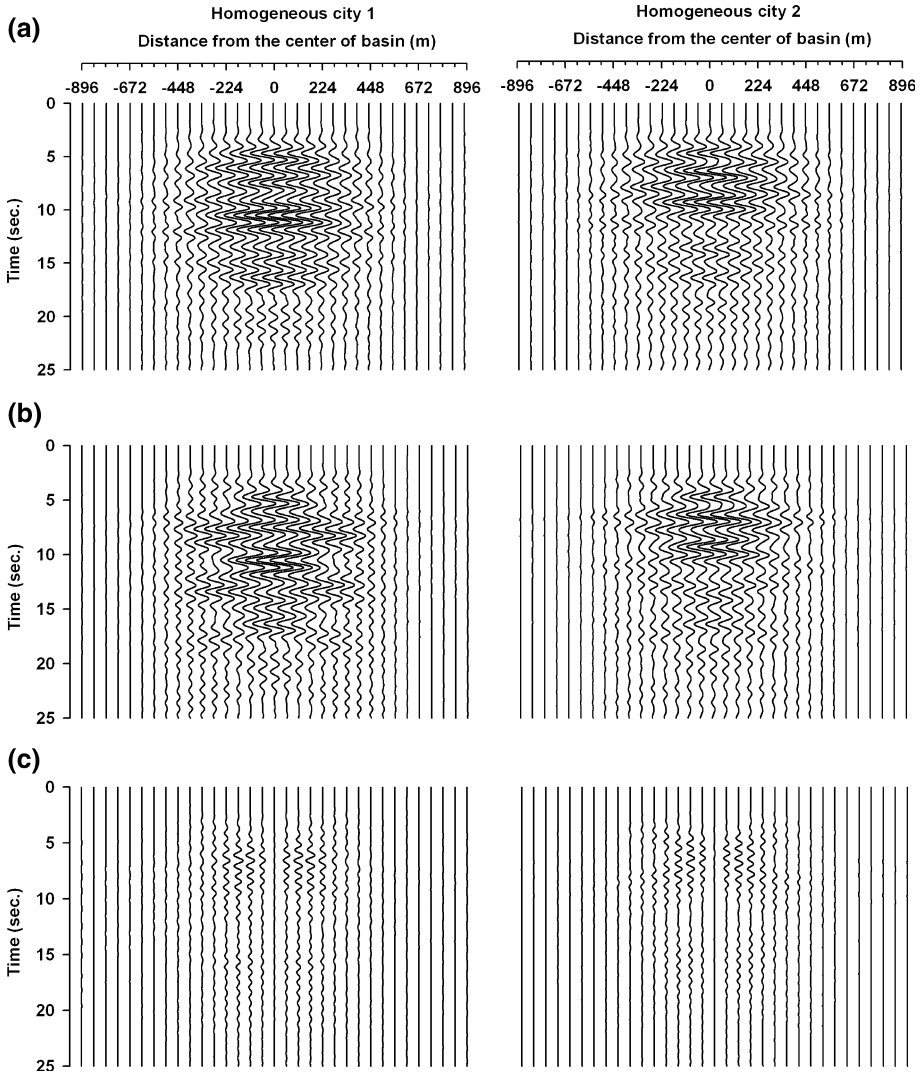

Fig. 6 Perturbations of the ground motions due to the SCI effect as compared to the free-field motion in the SS basin associated with homogeneous city 1 (*left*) and city 2 (*right*).(Note: the value of normalization factor used is just half of that used in Figs. 4 and 5). **a** NS component of NS array. **b** NS component of EW array. **c** UD component of NS array

with and without city 1 and city 2 in the SS and TRP basins at four locations (at distances of 0.0, 224, 448 and 672 m from the centre of the basin) is shown in Figs. 10 and 11, respectively. An analysis of Figs. 10 and 11 reveals the reduction in ground motion amplification because of the SCI effects. The largest reduction in spectral amplification (56.7 %) occurs at around 0.6 Hz for city 1 at the centre of the basins, which is the considered F_o of the B16 building as well as the lowest F_0 of the SS basin. In case of homogenous city 2, the largest reduction in spectral amplification (48.4 %) is also around the lowest F_o of the SS basin. On the other hand, the reduction in spectral amplifications at

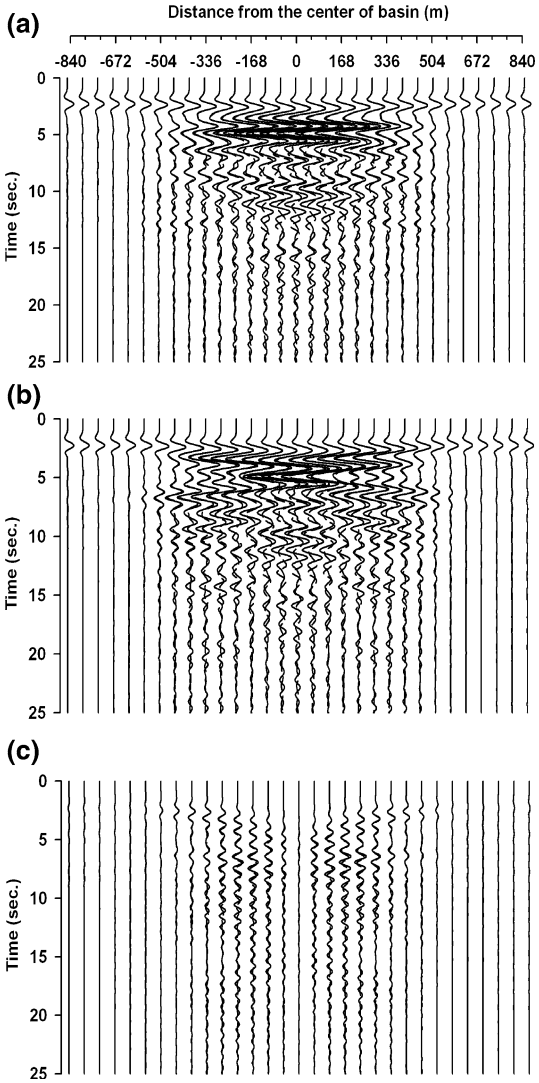

Fig. 7 A comparison of ground motions in different components corresponding to with (*dashed line*) and without (*solid line*) homogenous city 1 in TRP basin. **a** NS component of NS array. **b** NS component of EW array. **c** UD component of NS array

the centre of the TRP basin at around the 0.6 Hz in city 1 and city 2 is 22 and 39.1 %, respectively. The % reduction in spectral amplification for city 2 is observed to be 44.8 and 37.5 % at the fundament frequency (1.2 Hz) of B8 building in SS and TRP basin, respectively. The largest % reduction in the spectral amplifications in the SS basin may be due to the large amplification of ground motion caused by the focusing of the BGS waves in the central part of the SS basin. Figure 12a–c depicts the comparison of spatial variation of % reduction in largest amplitude (left), the kinetic energy (centre) and average spectral amplification (ASA) (right) in the homogeneous city 1 and city 2 with respect to the free-field motion in the SS basin in different components along the NS and EW arrays. The kinetic energy (KE) was computed using the following relationship.

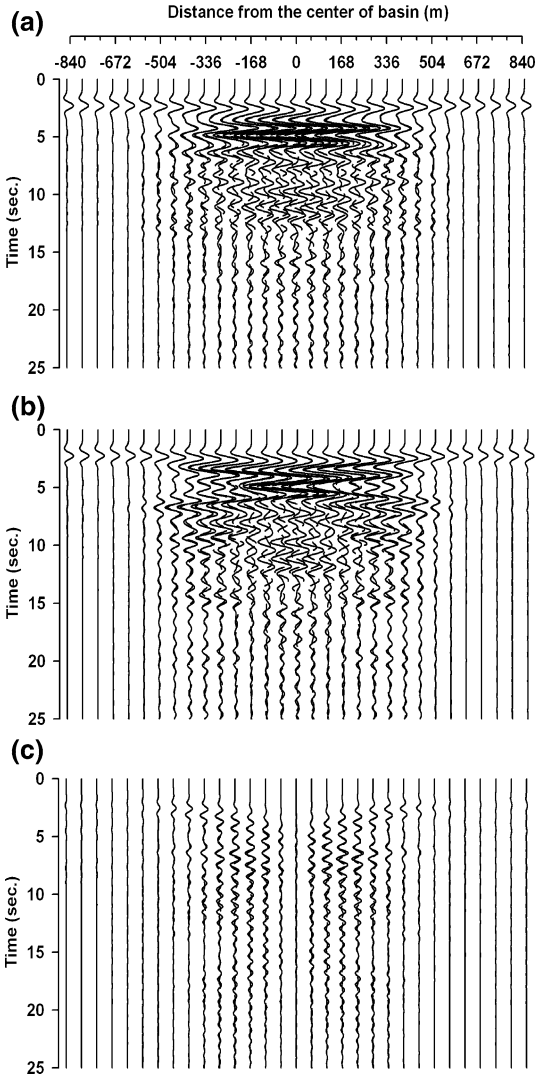

Fig. 8 A comparison of ground motions in different components corresponding to with (*dashed line*) and without (*solid line*) homogenous city 2 in TRP basin. **a** NS component of NS array. **b** NS component of EW array. **c** UD component of NS array

$$\mathrm{KE} = \frac{1}{T}\int_0^{\mathrm{T}} |\mathrm{v}(\mathrm{x},\mathrm{t})|^2 \mathrm{dt}$$

where T is the signal duration and v(x,t) is the particle velocity. The ASA is computed using the average of ratio of spectra of different recorded components in basins with the spectra of NS component of the response of model with no basin. Similarly, Fig. 13a–c depicts the comparison of spatial variation of % reduction in largest amplitude (left), the kinetic energy (centre) and average spectral amplification (ASA) (right) in the homogeneous city 1 and city 2 with respect to the free-field motion in the TRP basin in different components along the NS and EW arrays.

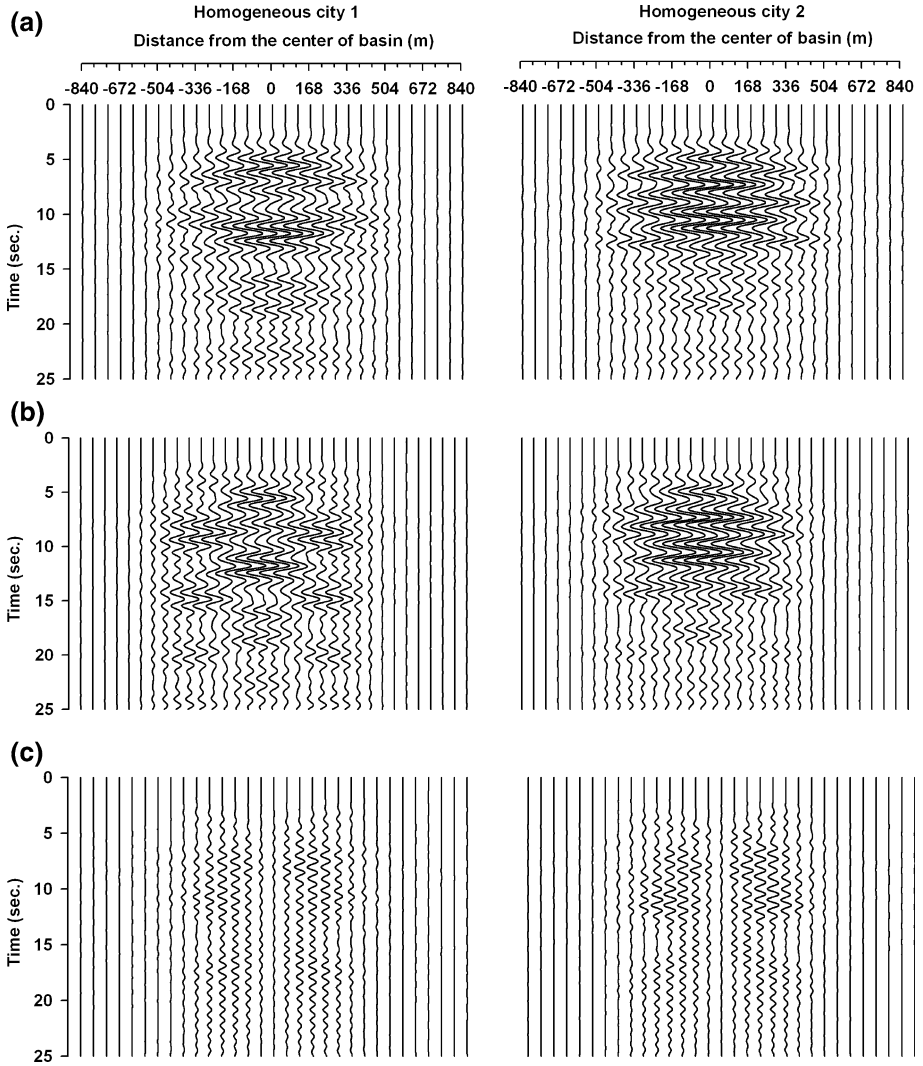

Fig. 9 Perturbations of the ground motions due to the SCI effect as compared to the free-field motion in the TRP basin associated with homogeneous city 1 (*left*) and city 2 (*right*). (Note: the value of normalization factor used is just half of that used in Figs. 7 and 8). **a** NS component of NS array. **b** NS component of EW array. **c** UD component of NS array

The reduction in maximum amplitude due to the SCI in the homogenous city 1 situated in SS basin is 13.2, 13.6 and 29.5 % in NS component of NS and EW arrays and UD component of NS array, respectively. On the other hand, the reduction in maximum amplitude in the homogenous city 2 is 16.0, 16.0 and 29.7 %. The minor increase in amplitude (around 5 %) at the receivers outside of both the cities is also inferred. The reduction in KE due to the SCI in the homogenous city 1 is 36.0, 34.0 and 47.0 % and in the homogeneous city 2 is 42.1, 42.1 and 58.7 % in NS component of NS and EW arrays and UD component of NS array, respectively. Similarly, the reduction in ASA due to SCI

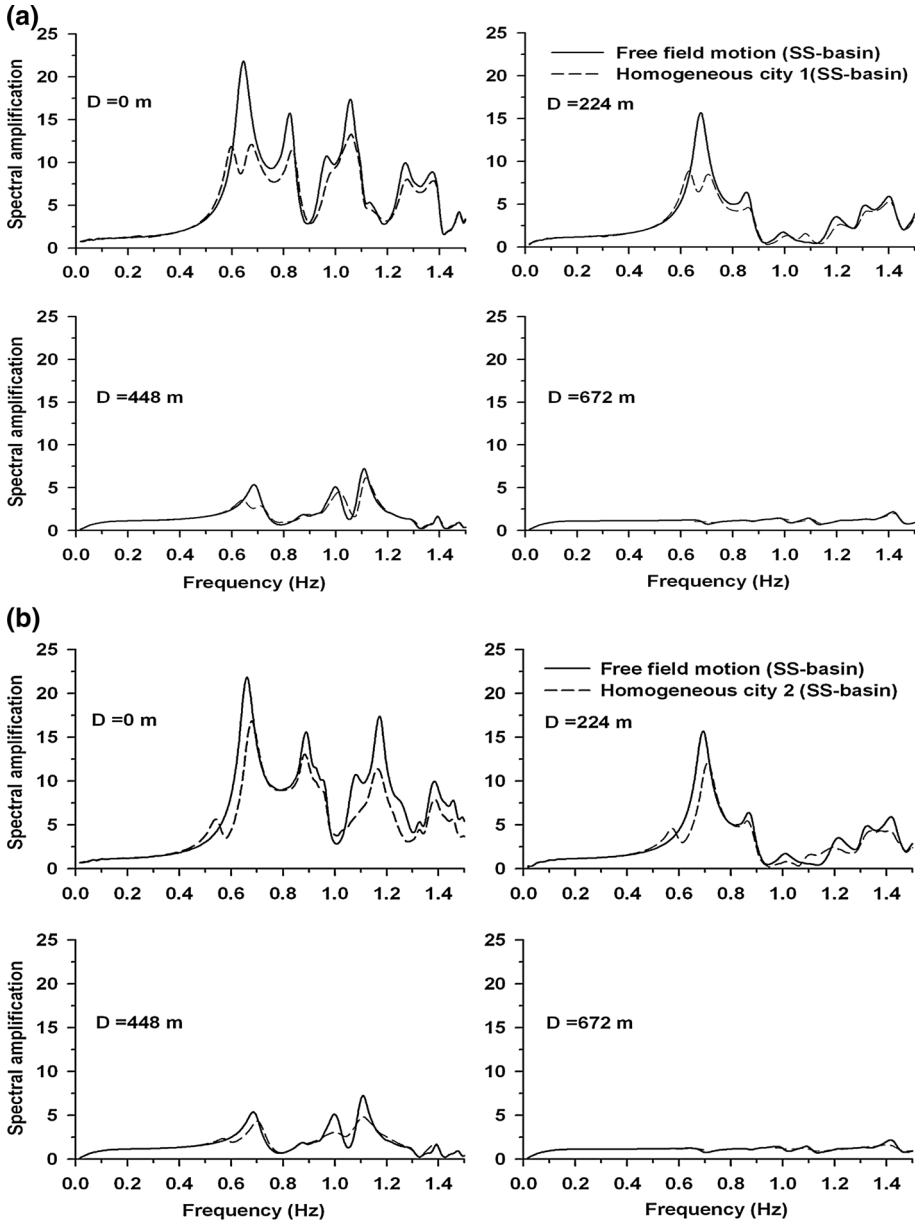

Fig. 10 A comparison of spectral amplifications of the NS component of the NS array at four locations in **a** homogeneous city 1 and **b** city 2, respectively, with the free-field motion in the SS basin

in the homogeneous city 1 is 14.0, 14.0 and 21.4 % and in city 2 is 18.7, 18.7 and 28.2 % in NS component of NS and EW arrays and UD component of NS array, respectively. Similarly, the reduction in maximum amplitude due to the SCI in the homogenous city 1 situated in trapezoidal basin is 11.6, 11.7 and 13.5 % in NS component of NS and EW

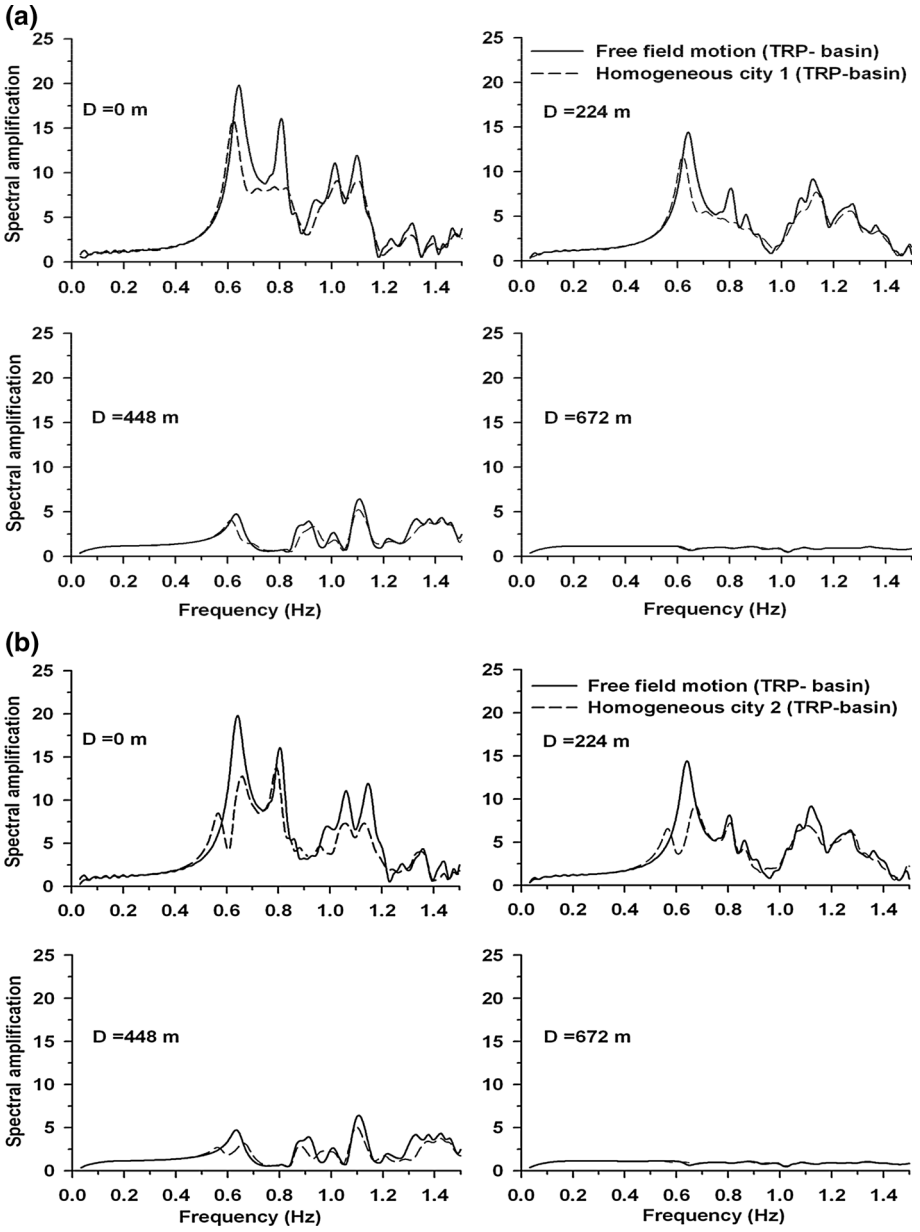

Fig. 11 A comparison of spectral amplifications of the NS component of the NS array at four locations in **a** homogeneous city 1 and **b** city 2, respectively, with the free-field motion in the TRP basin

arrays and UD component of NS array, respectively. On the other hand, the reduction in maximum amplitude in the homogenous city 2 is 15.8, 16.0 and 20.7 %. The reduction in KE due to the SCI in the homogenous city 1 is 34.8, 34.8 and 59.5 % and in the city 2 is 39.8, 40.2 and 59.5 % in NS component of NS and EW arrays and UD component of NS

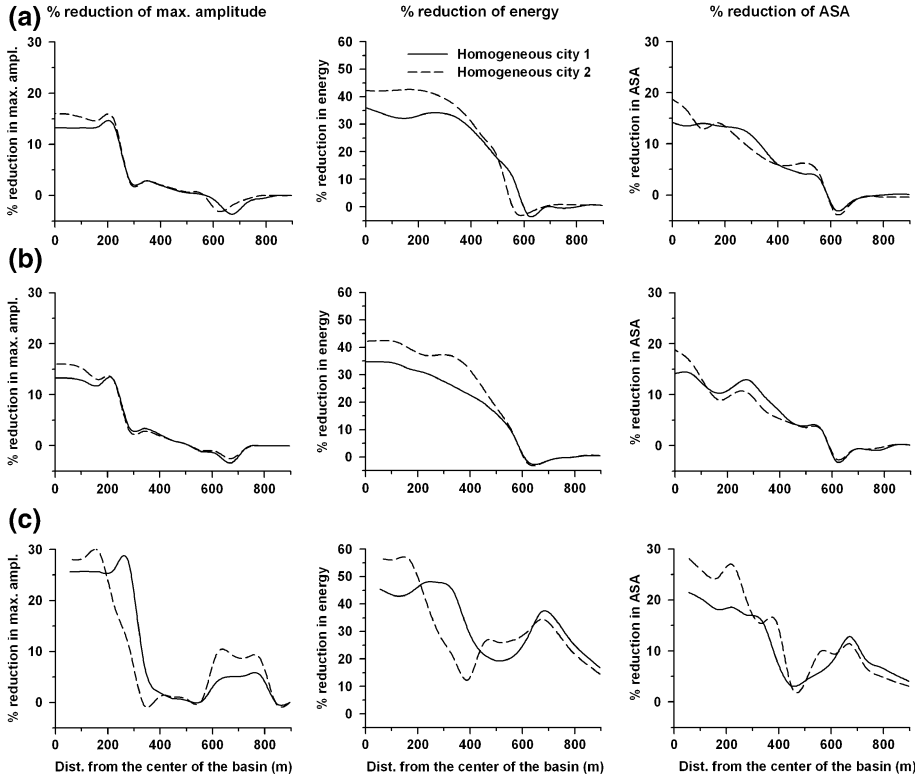

Fig. 12 A comparison of % reduction in maximum recorded amplitude, kinetic energy and ASA due to homogeneous city 1 and city 2 along the **a** NS component of NS array, **b** NS component of EW array and **c** UD component of NS array, respectively, with respect to free-field motion in the SS basin

array, respectively. Similarly, the reduction in ASA due to SCI in the homogeneous city 1 is 14.7, 14.7 and 28.0 % and in city 2 is 18.9, 18.9 and 29.3 % in NS component of NS and EW arrays and UD component of NS array, respectively. Based on the analysis of Figs. 12 and 13, it can be inferred that the SCI effects in the SS basin are somewhat more than the TRP basin. Furthermore, the SCI effects are more due to city 2 as compared to the city 1, in both the basins. So it may be concluded that the SCI effects very much depend on both the building type in the city and the shape of the basin. It is also concluded that the SCI effect is considerably large if the fundamental frequency of buildings matches with the lowest fundamental frequency of the basin.

6 Sediment layering effects

To study the effect of sediment layers in the basin on the SCI effects, seismic responses of the SSL1-SSL3 models with single, double and triple sediment layers in the SS basin, respectively, were computed along the NS and EW arrays (SSL1 model is same as the SS basin model). The material properties of different sediment layers of the SSL1-SSL3 site city models are given in Table 3. Further, the quality factors for the P- and S-waves in

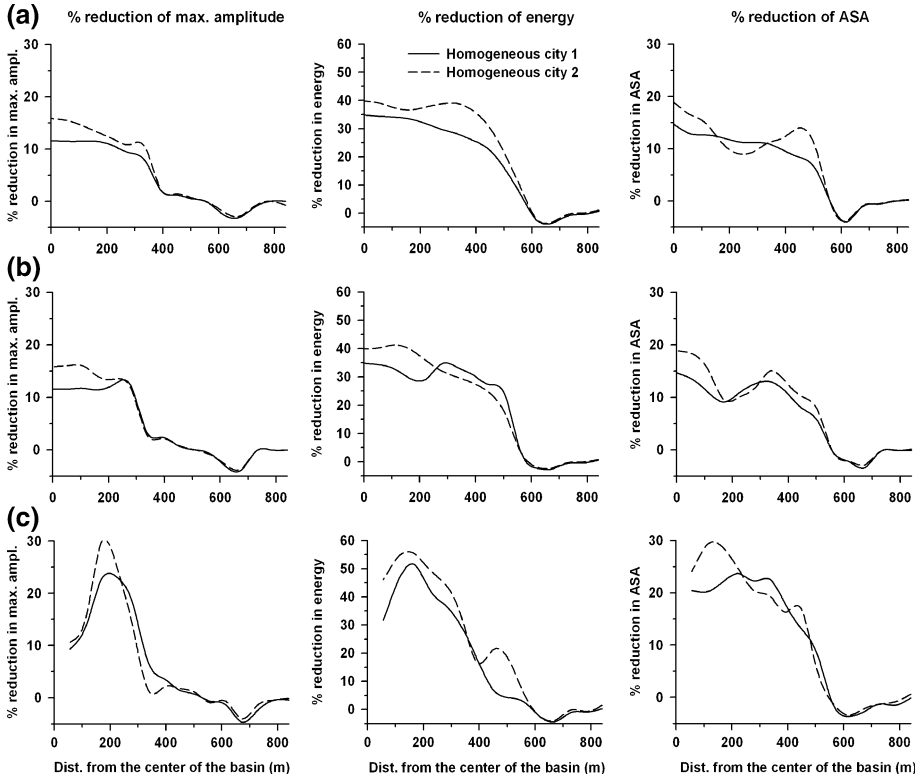

Fig. 13 A comparison of % reduction in maximum recorded amplitude, kinetic energy and ASA due to homogeneous city 1 and city 2 along the **a** NS component of NS array, **b** NS component of EW array and **c** UD component of NS array, respectively, with respect to free-field motion in the TRP basin

Table 3 Parameters for the sediment in SSL1-SSL3 basin models with single, double and triple soil layers

Basin model	V_S (m/s)			V_P (m/s)			Thickness (m)			Density (kg/m^3)		
	1st layer	2nd layer	3rd layer	1st layer	2nd layer	3rd layer	1st layer	2nd layer	3rd layer	1st layer	2nd layer	3rd layer
SSL1	360	–	–	612	–	–	150	–	–	1800	–	–
SSL2	288	432	–	489.6	734.4	–	60	90	–	1780	1813	–
SSL3	125	376.8	578	212.5	640.6	983	18	48	84	1700	1810	1815

different sediment layers at the reference frequency were taken as 10 % of the corresponding velocities in sediment layers. The seismic responses of the SSL2 and SSL3 basin models in the considered components along the NS and EW arrays without (solid line) and with (dashed line) homogeneous city 1 are shown in Figs. 14 and 15, respectively. An analysis of Figs. 4, 14 and 15 does not depict the expected increase in ground motion amplification due to the decrease in S-wave velocity in the upper most sediment layer of the basin, particularly in case of the BGS waves. A decrease in duration and amplitude of the BGS waves can be inferred with an increase in sediment layers. The perturbations in

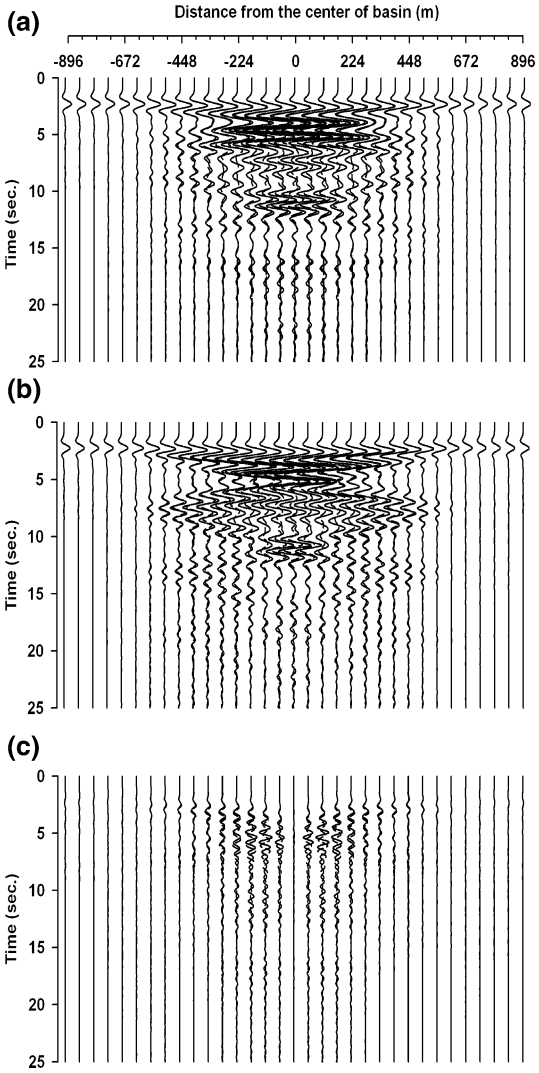

Fig. 14 A comparison of ground motions in different components corresponding to with (*dashed line*) and without (*solid line*) homogenous city 1 in SSL2 basin. **a** NS component of NS array. **b** NS component of EW array. **c** UD component of NS array

ground motion in different considered components along the NS and EW arrays in the SSL1, SSL2 and SSL3 models are shown in Fig. 6 (left panel), Fig. 16 (left panel) and Fig. 16 (right panel), respectively. The analysis of Figs. 6 and 16 depicts overall decrease in perturbation with an increase in sediment layers except in the horizontal components of ground motion in the central part of the basins.

Figure 17a–c shows the spatial variation in the percentage reduction in the largest amplitude, kinetic energy and ASA with respect to the free-field, respectively, due to the SCI effects in the SSL1-SSL3 basins. An analysis of Fig. 17 reveals that the SCI effect is increasing with an increase in sediment layer, in the central part of in the SS basin and reverse is the case in the outer part of the SS basin. For example, the largest % reduction in ASA at the centre of SSL1-SSL3 basin models is 14.7, 24.6 and 40.8 %, respectively, and the same at a distance of 450 m from the centre of basin is 4.7, 1.7 and 0.5 %, respectively.

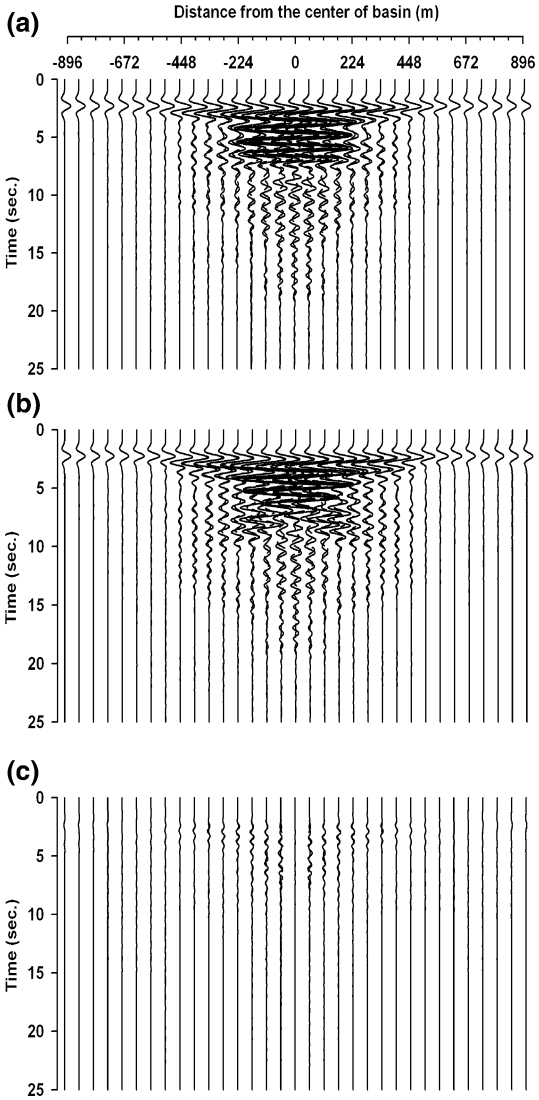

Fig. 15 A comparison of ground motions in different components corresponding to with (*dashed line*) and without (*solid line*) homogenous city 1 in SSL3 basin. **a** NS component of NS array. **b** NS component of EW array. **c** UD component of NS array

So, it is concluded that the sediment layering increases the % reduction in ASA due to the SCI effects in the central part and decreases in the outer part of the SS basin/city. It may be due to the larger damping in the top layer/layers in the SSL2 and SSL3 basin models.

7 City shape effects

To study the role of city shape in the SCI effects on the ground motion characteristics, a city model with four-hubs of B16 buildings, as shown in Fig. 18, was considered. The four-hub city model containing 320 B16 buildings (80 buildings in each hub) is situated in the SS basin. The total surface area (589,568 m^2) and the city density (0.42) for the four-hub

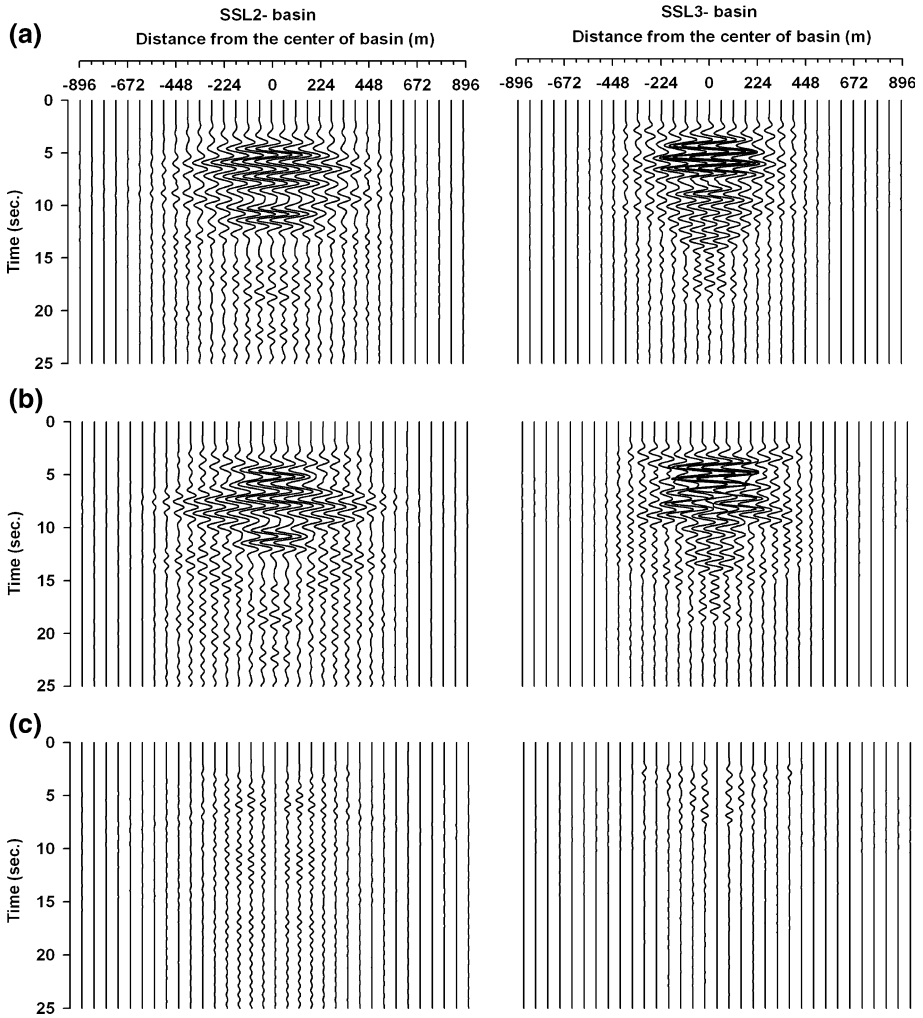

Fig. 16 Perturbations of the ground motions due to the SCI effect of homogeneous city 1 as compared to the free-field motion in the SSL1 basin (*left*) and SSL2 basin (*right*). (Note: the value of normalization factor used is just half of that used in Figs. 14 and 15). **a** NS component of NS array. **b** NS component of EW array. **c** UD component of NS array

city are approximately same as for the homogeneous city 1. The seismic responses were computed at the NS and EW arrays. Figure 19a shows the comparison of the spatial variations of ASA in NS components along the NS array in case of the four-hub city with the homogeneous city 1 and the free-field motion. Similarly, Fig. 19b reveals the % reduction in ASA due to the SCI effects associated with the four-hub city and homogeneous city 1 as compared to the free-field motion. The analysis of Fig. 19 depicts that the SCI effects in case of the four-hub city is lesser than the homogeneous city 1. The obtained largest percentage reduction in the ASA in case of four-hub city and city 1 is 12.1 and 14.2 %, respectively. Further, the largest % reduction in ASA in case of four-hub city is not occurring at the centre of the SS basin, it is at an offset of 200 m. But it is interesting to

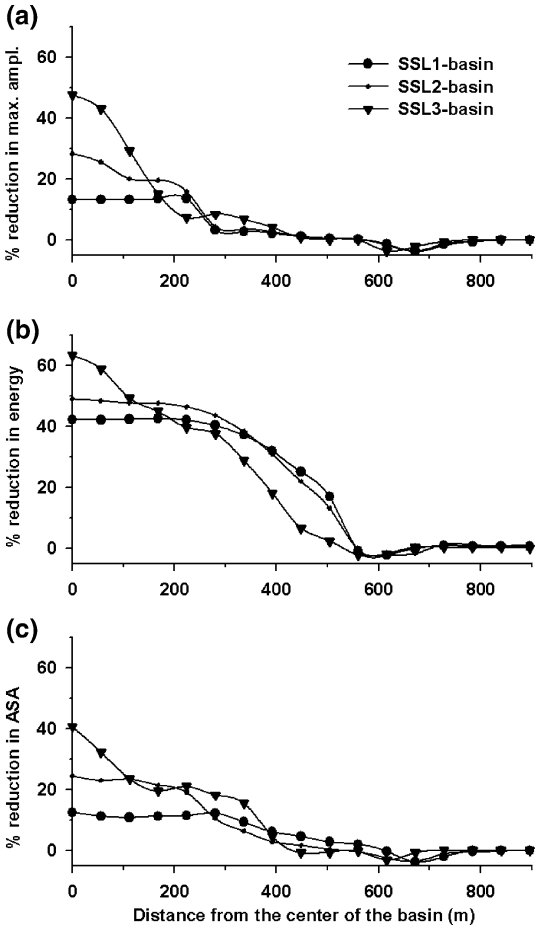

Fig. 17 **a–c**. A comparison of % reduction in maximum recorded amplitude, kinetic energy and ASA in the NS component of the NS array due to the homogeneous city 1 situated in the SSL1, SSL2 and SSL3 basins, respectively, with respect to the free-field motion in the respective basins

note that in case of the four-hub city, none of the buildings are falling in the path of the body waves and surface waves propagating along the considered arrays for the recording (Fig. 18) and a reduction in ASA of the order of 10.2 % is near the centre of the SS basin. It is further interesting to note that the % reduction in ASA in case of four-hub city is comparable with the city 1 in some part of the SS basin (around 450 m from the centre of the basin). So it can be inferred that the obtained % level of reduction in ground motion is mainly due to the effects of buildings on the BGS waves, which are propagating in infinite elliptical planes from basin edge to the centre of the SS basin.

8 City density effects

To study the role of city density (CD) in the SCI effects, the seismic responses of the homogeneous city 1 and city 2 situated in the SS basin were computed for different CD. The four city density models C1CD1–C1CD4 for homogeneous city 1 having number of B16 buildings as 324, 432, 480 and 576, respectively, were considered. So, the CD for the

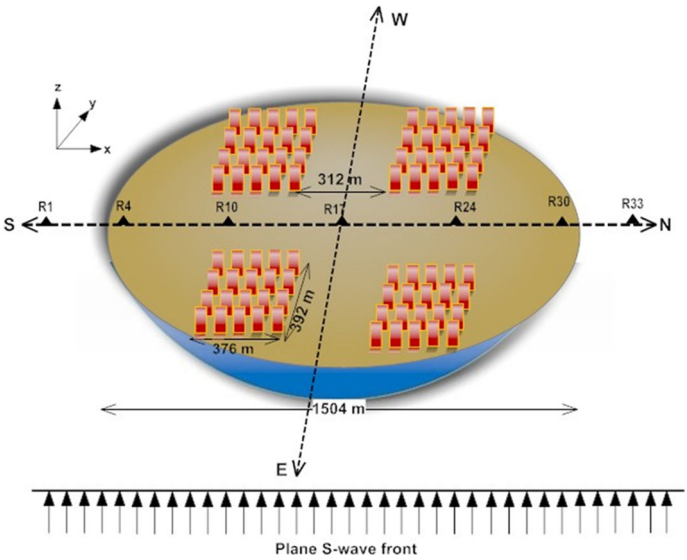

Fig. 18 A model with four-hub city of the B16 buildings situated in the SS basin

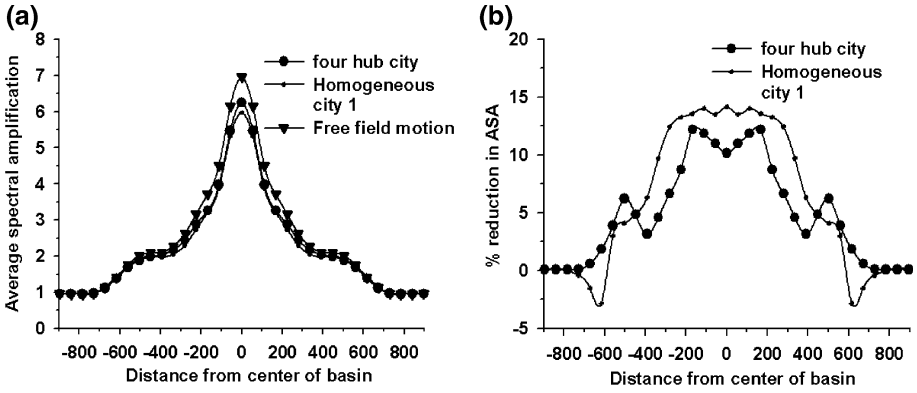

Fig. 19 **a** A comparison of ASA in the four-hub city and homogeneous city 1 with the free-field motion in the SS basin and **b** comparison of % reduction in ASA in the four-hub city and homogeneous city 1 with respect to the free-field motion in the SS basin

C1CD1–C1CD4 models is 0.42, 0.56, 0.63 and 0.75, respectively. Similarly, the three city density models C2CD1–C2CD3 for the homogeneous city 2 having number of B8 buildings as 624, 840 and 960, respectively, were considered. The CD for the C2CD1–C2CD3 models is 0.42, 0.56, and 0.63, respectively. Further, the surface area of all the city density models of city 1 and city 2 is 776 × 776 m^2. Figure 20a, b (left) depicts the comparison of spatial variation of ASA for the C1CD1–C1CD4 city density models in the NS components along the NS and EW arrays, respectively, with corresponding free-field motion. A decrease in ASA with an increase in city density can be inferred in both the components. It is also inferred from these figures that the reduction in ASA is more for NS component of EW array (means the array along which the only Love is propagating). Figure 20a, b

(right) depicts the comparison of spatial variation of % reduction in ASA for the C1CD1–C1CD4 city density models in the NS components along the NS and EW arrays, respectively, with respect to the free-field motion. The obtained largest decrease in ASA is 22 and 27 % in NS components of NS and EW arrays respectively for the C1CD4 city density model is at the centre of the SS basin.

Similarly, Fig. 21a, b (left) depicts the comparison of spatial variation of ASA for the C2CD1–C2CD3 city density models in the NS components along the NS and EW arrays, respectively, with corresponding free-field motion. A decrease in ASA with an increase in city density can be inferred in both the components. It is also inferred from these figures that the reduction in ASA is more for NS component of EW array. Figure 21a, b (right) depicts the comparison of spatial variation of % reduction in ASA for the C2CD1–C2CD3 city density models in the NS components along the NS and EW arrays, respectively, with respect to the free-field motion. The obtained largest decrease in ASA is 29 and 32 % in NS components of NS and EW arrays, respectively, for the C2CD3 city density model is at the centre of the SS basin. The analysis of Figs. 20 and 21 depicts that the SCI effects very much depend on the city density and an increase in this effects with city density can be inferred in both the considered cities. However, the city density effect was more in city 2 as compared to the city 1. For example, largest % decrease in ASA in case of

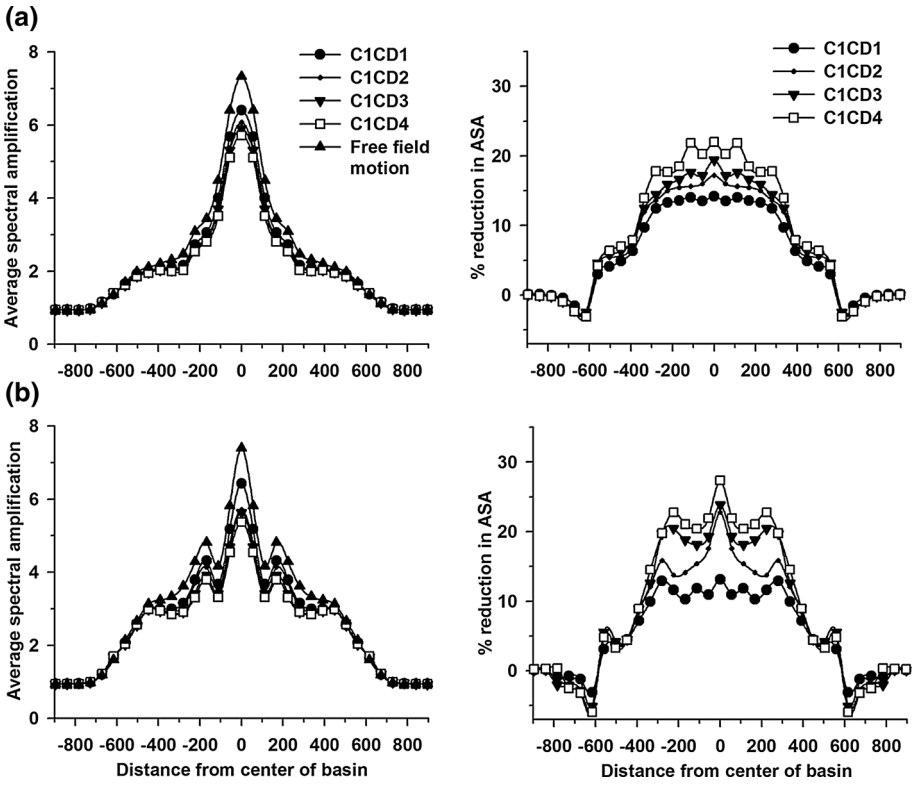

Fig. 20 A comparison of ASA (*left*) and % reduction in ASA (*right*) in homogeneous city 1 for different city density with respect to the free-field motion in the SS basin in the **a** NS component of NS array and **b** NS component of EW array, respectively

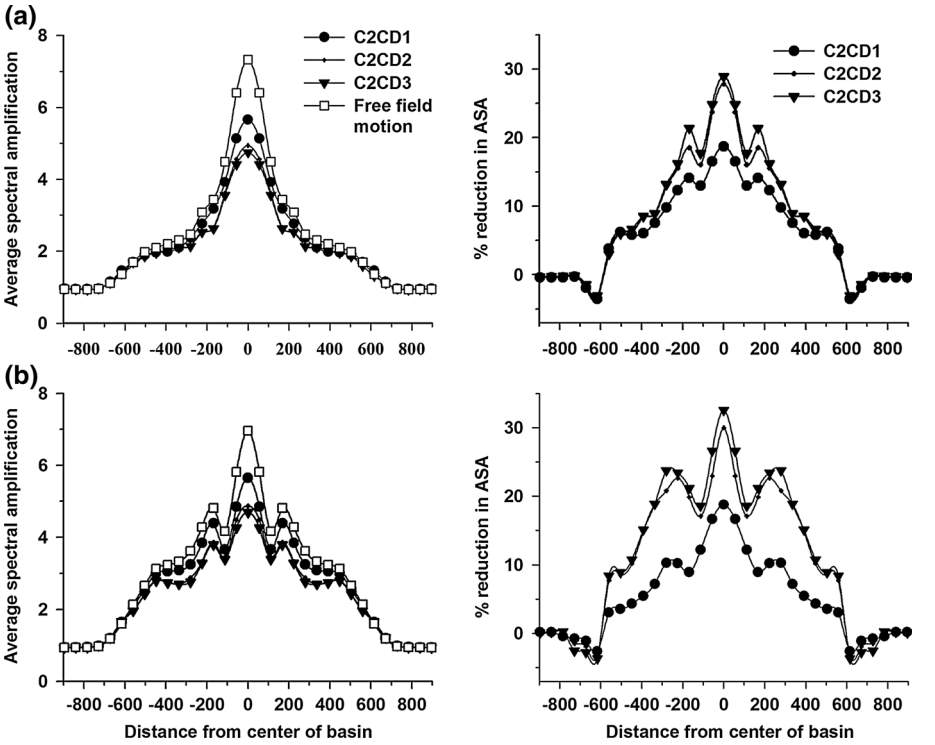

Fig. 21 A comparison of ASA (*left*) and % reduction in ASA (*right*) in homogeneous city 2 for different city density with respect to the free-field motion in the SS basin in the **a** NS component of NS array and **b** NS component of EW array, respectively

C1CD3 and C2CD3 with same city density as 0.63 along the EW array was 21 and 32 %, respectively. Furthermore, it appears that the city density effect on ground motion reduction is increasing towards the centre of the SS basin.

9 Discussion

The analysis of responses at the top of the single B16, B12 and B8 buildings in the SS basin revealed that the first spectral amplification peak frequencies are very much corroborating with the fundamental frequency of the material between the top of the building and the base of the sediment. But, in case of B8 building, it is occurring at somewhat higher frequency. It may be due to the closeness of the fundamental frequency of the combined basin-building system with the fundamental frequency of the basin and the dominant frequency in the input signal. But such type of spectral amplification peak was not reported in case of the SH-wave modelling of SCI effects (Sahar et al. 2015). This needs further detailed study. The second spectral amplification peak frequency is occurring very near the fundamental frequency of the basin. However, in case of B8 building, very large spectral amplification of the order of 49 is occurring near 0.62 Hz. Although theoretically the largest spectral amplification should occur in case of the B16 building, the

assigned fundamental frequency for B16 building was matching with the fundamental frequency of the basin. The obtained % reduction in spectral amplification at the top of a building of city 2 as compared to the same at top of a single B8 building was 44.2 %. Similarly, the obtained % reduction in spectral amplification at the top of a building of city 1 as compared to the same at top of a single B16 building was 37.5 %. These findings very much corroborate with the findings of Kham et al. (2006) who reported through 2D basin-city models that the SCI effect is large when the soil frequency matches with the building frequency.

The analysis of ground motion perturbations, spatial variations of % reduction in peak amplitude, ASA and kinetic energy caused by the presence of city 1 and city 2 in the SS and TRP basins revealed that basin shape play an important role in the SCI effects. Based on the analysis of responses of the four-hub city, it may be concluded that the city 1 is beneficial to some extent as compared to the four-hub city, even though both the cities have same city density and building type. The analysis of different city density models reveals that the city density is a prominent parameter of the SCI, which largely reduces the ground motion amplitude in the city. For example, city density of city 1 increases from 0.42 to 0.75 which leads to a decrease in ASA from 14 to 27 %. On the other hand, city density of city 2 increases from 0.42 to 0.63 which leads to a decrease in ASA from 18.8 to 32.5 %. Further, in case of city which is under double resonance, an increase in city density from 0.42 to 0.63 has caused a decrease in KE from 40 to 69 %. Based on the 2D basin-city model simulations, Kham et al. (2006) reported that building density increases from 0.2 to 0.66 which leads to an energy decrease from 20 to 50 % under double resonance. It reflects that the SCI effects in 3D basin-city model may be much larger to that in a 2D basin-city model.

10 Conclusions

The role of 3D basin shape, sediment layers, city type, city shape and city density in the SCI effects on the free surface ground motion is studied in details. An analysis of responses of single B8, B12 and B16 buildings situated at the centre of the SS basin revealed the matching of the first spectral amplification peak frequency with the fundamental frequency of the combined basin-building system. The obtained very large amplification of the order of 49 for 0.62 Hz at the top of the B8 building may be due to the closeness of the fundamental frequency of the combined basin-building system with the fundamental frequency of basin and the dominant frequency in the used Ricker wavelet. The obtained largest spectral amplification reduction (44.2 %) at the top of a building of city 2 as compared to the same at the top of a single B8 building in the SS basin may also be due to the above phenomenon. The obtained very large reduction in spectral amplification in city 1 at the double resonance also corroborates with the findings of Kham et al. (2006) and Semblat et al. (2008).

The analysis of various 3D basin-city models revealed the very large role of basin shape, sediment layering, buildings in city, city shape and city density in the SCI effects on the free-field motion. The SCI effect was somewhat larger in the SS basin as compared the TRP basin. An increase in sediment layering in basin increases the % reduction in ASA as compared to the free-field motion due to SCI effects in the central part and decreases in the outer part of the SS basin. The obtained larger reduction in ASA in the city 1 as compared to the four-hub city, although the number of buildings and city density was similar,

revealed that the SCI effects also depend on the city shape. The obtained reduction in ASA in the four-hub city may be mainly due to the effects of city on the BGS waves since there are no buildings situated in the path of both the body waves and the BGS waves propagating along the considered arrays. An increase in % reduction in KE and ASA with an increase in city density in both the city 1 and city 2 was obtained. Further, in case of city 2, an increase in city density from 0.42 to 0.63 has caused a decrease in KE from 40 to 69 %.

Acknowledgments The second author is grateful to the Ministry of Earth Sciences, New Delhi, for financial assistance through Grant Number MES-484-EQD.

References

Bard PY, Bouchon M (1980) The seismic response of sediment filled valley, Part- I. The case of incident of SH waves. Bull Seismol Soc Am 70:1263–1286

Boutin C, Roussillon P (2004) Assessment of the urbanization effect on seismic response. Bull Seismol Soc Am 94(1):251–268

Chaljub E, Moczo P, Tsuno S, Bard PY, Kristek J, Kaser M, Stupazzini M, Kristekova M (2010) Quantitative comparison of four numerical predictions of 3D ground motion in the Grenoble Valley, France. Bull Seismol Soc Am 100:1427–1455

Chavez-Garcia FJ, Cardenas-Soto M (2002) The contribution of the built environment to the free-field ground motion in Mexico City. Soil Dyn Earthq Eng 22:773–780

Clouteau D, Aubry D (2001) Modification of ground motion in dense urban areas. J Comput Acoust 6:1659–1675

Cornou C, Gueguen P, Bard PY, Haghshenas E (2004) Ambient noise energy bursts observation and modeling: trapping of harmonic structure-soil induced–waves in a topmost sedimentary layer. J Seismol 8(4):507–524

Emmerich H, Korn M (1987) Incorporation of attenuation into time-domain computations of seismic wave fields. Geophysics 52:1252–1264

Foutch DA and Housner GW (1977) Observed changes in the natural periods of vibration of a nine story steel framed building. In: 6th WCEE, pp 2698–2704

Gallipoli MR, Mucciarelli M, Castro RR, Monachesi G, Contri P (2004) Structure, soil-structure response and effects of damage based on observations of horizontal-to-vertical spectral ratios of microtremors. Soil Dyn Earthq Eng 24:487–495

Gao S, Liu H, Davis PM, Knopoff GL (1996) Localized amplification of seismic waves and correlation with damage due to the Northridge earthquake. Bull Seismol Soc Am 86:S209–s230

Groby JP, Tsogka C, Wirgin A (2005) Simulation of seismic response in a city-like environment. Soil Dyn Earthq Eng 25(7–10):487–504

Gueguen P, Bard PY (2005) Soil-structure and soil-structure-soil interaction: experimental evidence at the Volvi test site. J Earthq Eng 9(5):657–693

Gueguen P, Bard PY, Oliveira CS (2000) Experimental and numerical analysis of soil motion caused by free vibration of a building model. Bull Seismol Soc Am 90:1464–1479

Guéguen P, Bard PY, Chavez-Garcia FJ (2002) Site-city interaction in Mexico City-like environments: an analytical study. Bull Seismol Soc Am 92(2):794–811

IS-1893 (Part 1) (2002) Criteria for earthquake resistant design of structures—Part 1: General provision and buildings. Bureau of Indian Standards

Israeli M, Orszag SA (1981) Approximation of radiation boundary conditions. J Comp Phys 41:115–135

Jennings PC (1970) Distant motion from a building vibration test. Bull Seismol Soc Am 60:2037–2043

Kamal, Narayan JP (2015) 3D basin-shape ratio effects on frequency content and spectral amplitudes of basin-generated surface waves and associated spatial ground motion amplification and differential ground motion. J Seismol. doi:10.1007/s10950-014-9466-8

Kanamori H, Mori J, Anderson DL, Heaton TH (1991) Seismic excitation by the space shuttle Columbia. Nature 349:781–782

Kham M, Semblat JF, Bard PY, Dangla P (2006) Seismic site–city interaction: main governing phenomena through simplified numerical models. Bull Seismol Soc Am 96:1934–1951

Kim WY, Sykes LR, Armitage JH, Xie JK, Jacob KH, Richards PG, West M, Waldhauser F, Armbruster J, Seeber L, Du WX, Lerner-Lam A (2001) Seismic waves generated by aircraft impacts and building

collapses at World Trade Center, New York City. Eos Trans Am Geophys Union 82(47):570–571. doi:10.1029/01EO00330
Kristek J, Moczo P (2003) Seismic wave propagation in viscoelastic media with material discontinuities- a 3D 4th order staggered grid finite difference modeling. Bull Seismol Soc Am 93:2273–2280
Kumar S, Narayan JP (2008) Implementation of absorbing boundary conditions in a 4th order accurate SH-wave staggered grid finite difference program with variable grid size. Acta Geophys 56:1090–1108
Merritt RG, Housner GW (1954) Effect of foundation compliance on earthquake stresses in multi-story buildings. Bull Seismol Soc Am 44:551–569
Moczo P, Kristek J, Vavrycuk V, Archuleta RJ, Halada L (2002) 3D heterogeneous staggered-grid finite-difference modelling of seismic motion with volume harmonic and arithmetic averaging of elastic moduli and densities. Bull Seismol Soc Am 92:3042–3066
Narayan JP (2005) Study of basin-edge effects on the ground motion characteristics using 2.5-D modeling. Pure Appl GEOPHYS 162:273–289
Narayan JP (2012) Effects of P-wave and S-wave impedance contrast on the characteristics of basin transduced Rayleigh waves. Pure Appl Geophys 169:693–709
Narayan JP, Kumar V (2014a) P-SV wave time-domain finite-difference algorithm with realistic damping and a combined study of effects of sediment rheology and basement focusing. Acta Geophys 62:1214–1245
Narayan JP, Kumar R (2014b) Spatial spectral amplification of basin-transduced rayleigh waves. Nat Hazards 71:751–765
Narayan JP, Sahar D (2014) 3D viscoelastic finite-difference code and modelling of basement focusing effects on ground motion characteristics. Comput Geosci. doi:10.1007/s10596-014-9442-y
Narayan JP, Sharma ML, Kumar A (2002) A seismological report on the January 26, 2001 earthquake at Bhuj. India Seismol Res Lett 73:343–355
Sahar D, Narayan JP, Kumar N (2015) Study of role of basin-shape in the site-city-interaction effects on the ground motion characteristics. Nat Hazards. doi:10.1007/s11069-014-1366-2
Semblat JF, Kham M, Bard PY (2008) Seismic-wave propagation in alluvial basins and influence of site-city interaction. Bull Seismol Soc Am 98:2665–2678
Semblat JF, Lokmane N, Driad-Lebeau L, Bonnet G (2010) Local amplification of deep mining induced vibrations Part 2: Simulation of ground motion in a coal basin. Soil Dyn Earthq Eng 30(10):947–995
Stewart JP, Seed RB, Fenves GL (1999) Seismic soil-structure interaction in buildings, II: empirical findings. J Geotech Geo-environ Eng 125:38–48
Taborda R, Bielak J (2011) Large-scale earthquake simulation- Computational seismology and complex engineering systems. Comput Sci Eng 13:14–26. doi:10.1109/MCSE.2011.19
Tsogka C, Wirgin A (2003) Simulation of seismic response in an idealized city. Soil Dyn Earthq Eng 23:391–402
Wirgin A, Bard PY (1996) Effects of building on the duration and amplitude of ground motion in Mexico City. Bull Seismol Soc Am 86:914–920
Wolf JP (1985) Dynamic soil-structure interaction. Prentice-Hall Inc, Englewood Cliffs
Wong HL, Trifunac MD (1975) Two dimensional antiplane building-soil-building interaction for two or more buildings and for incident plane SH waves. Bull Seismol Soc Am 65:1863–1885
Zeng C, Xia J, Miller R, Tsoflias G (2012) An improved vacuum formulation for 2D finite-difference modeling of Rayleigh waves including surface topography and internal discontinuities. Geophysics 77:T1–T9